Simulations of Grain Refinement in Various Steels Using the Three-Scale Crystal Plasticity Model

KAROL FRYDRYCH

In this paper, the recently developed three-scale crystal plasticity model is applied to simulate microstructural evolution of austenitic and ferritic stainless steels subjected to large plastic strains. It is shown that the model is able to correctly predict both texture and misorientation angle distributions in the materials studied. Moreover, it can correctly capture the grain-refinement kinetics and the influence of the stacking fault energy. Finally, it is confirmed that the 3SCP model is a computationally attractive alternative for reliable modeling of microstructural evolutions in metals and alloys.

https://doi.org/10.1007/s11661-019-05373-z

I. INTRODUCTION

OBTAINING very small grains in polycrystalline metals and alloys has been attracting increasing attention of scientists and engineers mainly due to the involved improvement of the materials strength. Specifically, it was shown that the Hall–Petch relationship coupling the inverse of the square root of the grain size with the increasing yield strength is valid down to grain sizes as small as 10 to 25 nm.[1] Therefore, in the range of grain sizes attainable by conventional or severe plastic deformation processes, decreasing grain size should normally lead to considerable improvement in the strength.

Many authors studied the grain-refinement (GR) phenomenon occurring in severely deformed metals and alloys. However, most of the researchers were concerned with experiments and modeling of single-phase face-centered cubic (FCC) materials, such as copper and aluminum.[2,3] In such materials, grain refinement at large plastic strains can occur by continuous dynamic recrystallization (CDRX), where the misorientations between dislocation cells continuously increase leading to the formation of low- and high-angle grain boundaries (LABs and HABs). One should be careful not to mistake the CDRX with the ordinary or discontinuous dynamic recrystallization (DDRX) which is a process of nucleation and growth of new grains. For an extensive comparison and overview of CDRX and DDRX, see References 4 through 6.

On the other hand, considerably less attention was paid to grain refinement in steels, despite their wide range of industrial applications. It seems that there are two reasons for this situation. First, tracking the microstructural evolution in single-phase FCC metals is relatively easy due to small number of phenomena influencing the process. On the contrary, in steels, there can be single or multiple phases, with different crystallographic structures, *e.g.,* FCC austenite, body-centered cubic (BCC) ferrite and highly strained body-centered tetragonal martensite. This is challenging mainly from the point of view of the modeling. While it is not very hard to deal with single-phase FCC austenitic steel, considering microstructural evolution of dual-phase (DP) steels, especially in the presence of phase transformations, demands more effort. Second, the term "steel" covers a wide range of materials. Thus, it is much easier to compare studies by different groups conducted, *e.g.,* on copper (since it is a more or less similar material in every case) than to compare studies conducted on steel. One has to choose a particular steel, and there is little likelihood that a different group studied the same material.

The microstructural evolution in various stainless steels subjected to cold and warm deformation was experimentally studied in the series of papers by Belyakov *et al.*[7–15] These papers specifically deal with grain refinement by continuous dynamic recrystallization rather than the discontinuous one. In Reference 7, the effect of the initial microstructure upon the kinetics of GR in the 304-type austenitic steel (FCC) subjected to warm multiple compressions with a change of the direction of loading was analyzed. The authors concluded that grain refinement occurs faster when the initial grains are small and explained it by stating that the GR occurs near the grain boundaries. In smaller grains, more volume of the material is close to the boundaries, and thus, the GR can proceed more rapidly.

KAROL FRYDRYCH is with the Institute of Fundamental Technological Research (IPPT), Polish Academy of Sciences, Pawinskiego 5B, 02-106 Warsaw, Poland. Contact e-mail: kfryd@ippt.pan.pl.

Manuscript submitted February 21, 2019.
Article published online July 29, 2019

In Reference 8, the grain refinement occurring in two stainless steels subjected to rolling and swaging was analyzed. The authors concluded that the steel with an initial martensitic structure demonstrated faster kinetics of structural changes than the ferritic one. In Reference 9, the same deformation was applied to a DP stainless steel. In addition to more common microstructural evolution mechanisms, twinning and martensitic transformation in the austenite phase were observed.

An interesting analysis of the influence of the deformation route upon grain refinement was presented in Reference 10. The ferritic (BCC) stainless steel (Fe-15 pct Cr) was deformed both unidirectionally by rolling/swaging and by multidirectional compression. The grain-refinement kinetics in the case of the unidirectional deformation was found to be slightly faster. Also the grain shape was different, namely, the multidirectional deformation resulted in almost equiaxed grains, whereas the unidirectional elongation led to highly elongated grains. In References 12 and 15, the grain refinement in austenitic steels subjected to cold deformation was studied. However, contrary to Reference 7, twinning and martensitic transformation played a vital role in microstructural evolution in these materials. Thus, it can be seen that the mechanisms of grain refinement differ even inside the class of initially single-phase austenitic steels.

The grain refinement occurring as a result of CDRX was experimentally studied also by other groups of researchers, *cf. e.g.,* References 16 through 20 The microstructural evolution of the Ti-added interstitial-free (IF) steels subjected to accumulative roll bonding (ARB) was studied in References 16 through 18. The grain refinement in the austenitic Cr-Ni stainless steel subjected to cold multidirectional compression was studied in Reference 19, where it was assisted by martensitic transformation.

Modeling of the grain refinement received considerably less attention in the case of steels than in the case of, *e.g.,* pure FCC copper or aluminum (*cf.* References 2 and 5 for an overview). The focus of the present paper is on CDRX, and thus, only models dealing with such phenomena are cited below. In Reference 21, a qualitative model of grain refinement in BCC Armco iron was presented. The paper of Petryk *et al.*[22] describes the modeling of grain refinement in interstitial-free (IF) steel during multiaxis compression (MAXStrain®). The model developed in Reference 23 treats grain refinement through phenomenological equations. It enables one to trace the mean diameter of dislocation cells D_c, the mean spacing between parallel cell-block boundaries D_b and mean cell block width D_w. It works under the assumption that the decreases in D_c and D_b are slowed down due to the process of transformation of dislocation cell walls during reverse activation of slip systems on strain path reversals. However, in contrast to D_c and D_b, the evolution of D_w is governed by two terms: in addition to the one present for D_c and D_b, another one accounting for strain path complexity is present. This term is maximum when the applied direction of deformation is perpendicular to the direction of deformation before the strain path change. In addition, the model includes the calculated values of microstructural parameters in the hardening laws of macroscopic plasticity.

In Reference 24, the grain-refinement polycrystal model developed in Reference 25 was applied to simulate the grain size distribution, texture, and microstructure of the IF ferritic steel subjected to symmetric and asymmetric rolling. Good predictive capability of the model was shown. On the other hand, it should be noted that the model is very computationally intensive. An interesting approach to grain-refinement modeling is the application of the cellular automata. Frontal cellular automata were applied to the modeling of grain refinement in the high SFE microalloyed steel subjected to MAXStrain®deformation.[26] The distributions of disorientation angles were predicted using a model accounting for the formation of new low-angle grain boundaries and the rotation of the grains during the deformation.

The aim of the present paper is to show the capability of the recently developed computationally efficient three-scale crystal plasticity (3SCP) model to simulate microstructural evolutions in both FCC and BCC steels subjected to uni- and multidirectional deformation. After this introductory section, the structure of the model is briefly summarized in Section II. Section III presents the results of the simulations of microstructural evolution of the 304 austenitic stainless steel and Fe-15 pct Cr ferritic stainless steel. Finally, a discussion followed by conclusions is presented.

II. MODEL

The 3SCP model has been already described in References 2, 27, and 28. For convenience, it is briefly recalled here. The three-scale crystal plasticity model derives its name from the fact that three levels are present in the model, and the crystal plasticity model is applied to govern the behavior at the lowermost level. The levels are the *polycrystal*, the *metagrain*, and the *subgrain*. The specific crystallographic orientation is ascribed to each metagrain. The set of the orientations is chosen in accordance with the initial texture of the polycrystal. Here, due to lack of experimental data, a set of *NG* random orientations is ascribed to the metagrains. Then for each metagrain, a number *NS* of subgrain orientations is generated. Each subgrain orientation $\mathbf{Q}_i^g(0)$ is generated by rotating the initial orientation of the metagrain $\mathbf{Q}^g(0)$ around randomly generated axis $\mathbf{n}_i$ about randomly generated angle $\delta\psi_i(0) \in \langle 0, \Delta\psi \rangle$. The number of metagrains NG, the number of subgrains NS, and the maximum initial subgrain rotation angle $\Delta\psi$ can be thus considered as the parameters of the 3SCP model, which have to be specified together with the single crystal plasticity material parameters. Although $\Delta\psi$ can be treated as the 3SCP fitting parameter, its influence upon the results is rather small.

The idea of the model is to numerically represent the dislocation-induced cell substructure and then follow the evolution of subgrain orientations. The subgrains of similar orientations are expected to develop different

orientations due to the activation of different slip systems. The Taylor model in Reference 29 is used for the transition between the polycrystal and metagrain levels. The essence of the model is to enforce the same strain path in each grain (here: metagrain). Therefore, the strain redistribution to metagrains with "softer" orientations is not possible. Furthermore, the stress equilibrium between grains in the Taylor model is in general not satisfied. These reasons result in higher stress inhomogeneities between grains and the activation of higher number of slip systems compared with, *e.g.*, the Sachs[30] or the visco-plastic self-consistent (VPSC)[31,32] model.* The latter model is used for the transition between the levels of subgrain and metagrain. The "self-consistent" term in the name of the VPSC model is related to the fact that both the stress and strain equilibria between grains are satisfied. Since the model allows for the strain redistribution between grains (here: subgrains), the deformations of the individual subgrains can be achieved by smaller number of slip systems than that would be required by the Taylor model. Thus, each subgrain can deform by its own set of favorable slip systems, which leads to orientation splitting within metagrains. This was shown in Reference 2 to not be the case when using the VPSC model for both polycrystal–metagrain and metagrain–subgrain transitions. In such a case, the strain redistribution occurs on the polycrystal–metagrain level, and the metagrain is deformed on the strain path favorable for its orientation. The driving force for the activation of different slip systems in the individual subgrains belonging to the same metagrain is therefore considerably reduced.

*See References 33 and 34 for an overview of mean-field models.

In order to study the grain refinement, one can plot the overall texture of the material (using all orientations of subgrains) and study the misorientations between subgrains. The VPSC model used for the transition between subgrain and metagrain levels does not account for any neighborhood between subgrains, and thus, in order to calculate the misorientations, the neighboring subgrains are selected randomly. The misorientation angle $\delta\psi_{ij}^{g}(t)$ between subgrains i and j of the metagrain g at time step t is calculated as follows:[35]

$$2\cos(\delta\psi_{ij}^{g}) = \mathrm{tr}(\mathbf{R}_{ij}^{g}(t)) - 1, \qquad [1]$$

where

$$\mathbf{R}_{ij}^{g}(t) = \mathbf{Q}_{i}^{g}(t)\mathbf{Q}_{j}^{g}(t)^{T}. \qquad [2]$$

The single-crystal plasticity model described in References 2 and 36 is adopted here. The plastic deformation is assumed to be accommodated solely by slip, following[37]

$$\mathbf{L}^{p} = \sum_{\mathbf{r}=1}^{M} \dot{\gamma}^{r}\mathbf{m}^{\mathbf{r}} \otimes \mathbf{n}^{\mathbf{r}}, \quad \dot{\gamma}^{r} = v_0 \,\mathrm{sign}(\tau^{r})\left|\frac{\tau^{r}}{\tau_{c}^{r}}\right|^{n} \quad \tau^{r} = \mathbf{m}^{\mathbf{r}} \cdot \boldsymbol{\sigma} \cdot \mathbf{n}^{\mathbf{r}} \qquad [3]$$

where M is a number of slip systems; and τ^{r}, τ_{c}^{r} — resolved shear stresses on r system and its critical value, respectively; $\mathbf{m}^{\mathbf{r}}$ and $\mathbf{n}^{\mathbf{r}}$ are the unit vectors defining the slip system geometry; n is a rate sensitivity parameter; v_0 is a reference slip velocity; and $\boldsymbol{\sigma}$ is the Cauchy stress. The evolution of τ_{c} is governed by the following hardening model[38,39]:

$$\dot{\tau}_{c}^{r} = h_0\left(1 - \frac{\tau_{c}^{r}}{\tau_{\mathrm{sat}}}\right)^{\beta} \sum_{q=1}^{M} h_{rq}|\dot{\gamma}^{q}|, \quad h_{rq} = q + (1-q)|\mathbf{n}^{\mathbf{r}} \cdot \mathbf{n}^{\mathbf{q}}|. \qquad [4]$$

The parameters of the hardening model for each material studied will be specified in Section III.

III. RESULTS

The 3SCP simulations are performed as follows. First, the parameters of the crystal plasticity model are chosen in such a way that the predicted level of stress is approximately the same as in experiment. To this end, the two-scale crystal plasticity simulations for 500 random crystallographic orientations are performed. Next, the 3SCP simulation is conducted as described in Section II. The parameters of the 3SCP model itself are as follows: NG = 200, NS = 100, $\Delta\psi = 1.0$ deg.

A. *304 Austenitic Stainless Steel*

First, the simplest case of 304 austenitic stainless steel subjected to multiple compressions as in Reference 7 is simulated. The established set of parameters is shown in Table I. In this case, no twinning or strain-induced martensitic transformation was observed; therefore, in the modeling, it is assumed that plastic deformation occurs solely by dislocation slip on 12 independent $\{111\}\langle 110\rangle$ systems.

Figure 1 shows the misorientation angle distributions obtained in the 3SCP simulation. The histograms can be compared with Figure 11a in Reference 7. The results are qualitatively similar to the experimental data. Moreover, the predicted average misorientation angle is nearly the same as in the cited paper. The fraction of high-angle boundaries is also close to the experimental data.

B. *Fe-15 Pct Cr Ferritic Stainless Steel*

Next, two simulations of the microstructural evolution of the Fe-15 pct Cr ferritic alloy are conducted. The set of material parameters is presented in Table II. The plastic deformation is assumed to occur by slip on 12 independent $\{011\}\langle 11\bar{1}\rangle$ systems. Following Reference

Table I. The Established Single-Crystal Parameters of the 304 Austenitic Stainless Steel

τ_{c}^{0} (MPa)	τ_{sat} (MPa)	h_0	β	q	n
30	170	500	1.0	1.4	15

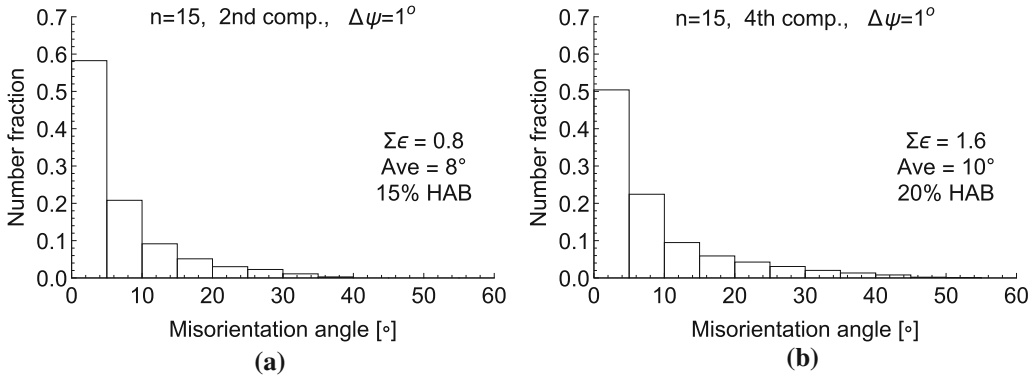

Fig. 1—The misorientation angle distributions calculated in the simulation of the multidirectional compression applied to 304 austenitic stainless steel after (*a*) 2 passes (0.8 strain) and (*b*) 4 passes (1.6 strain). The values of accumulated strain, average misorientation angle, and HAB fraction are shown in the plots.

Table II. The Established Single-Crystal Parameters of the Fe-15 pct Cr Binary Ferritic Alloy

τ_c^0 (MPa)	τ_{sat} (MPa)	h_0	β	q	n
80	150	300	1.0	1.4	20

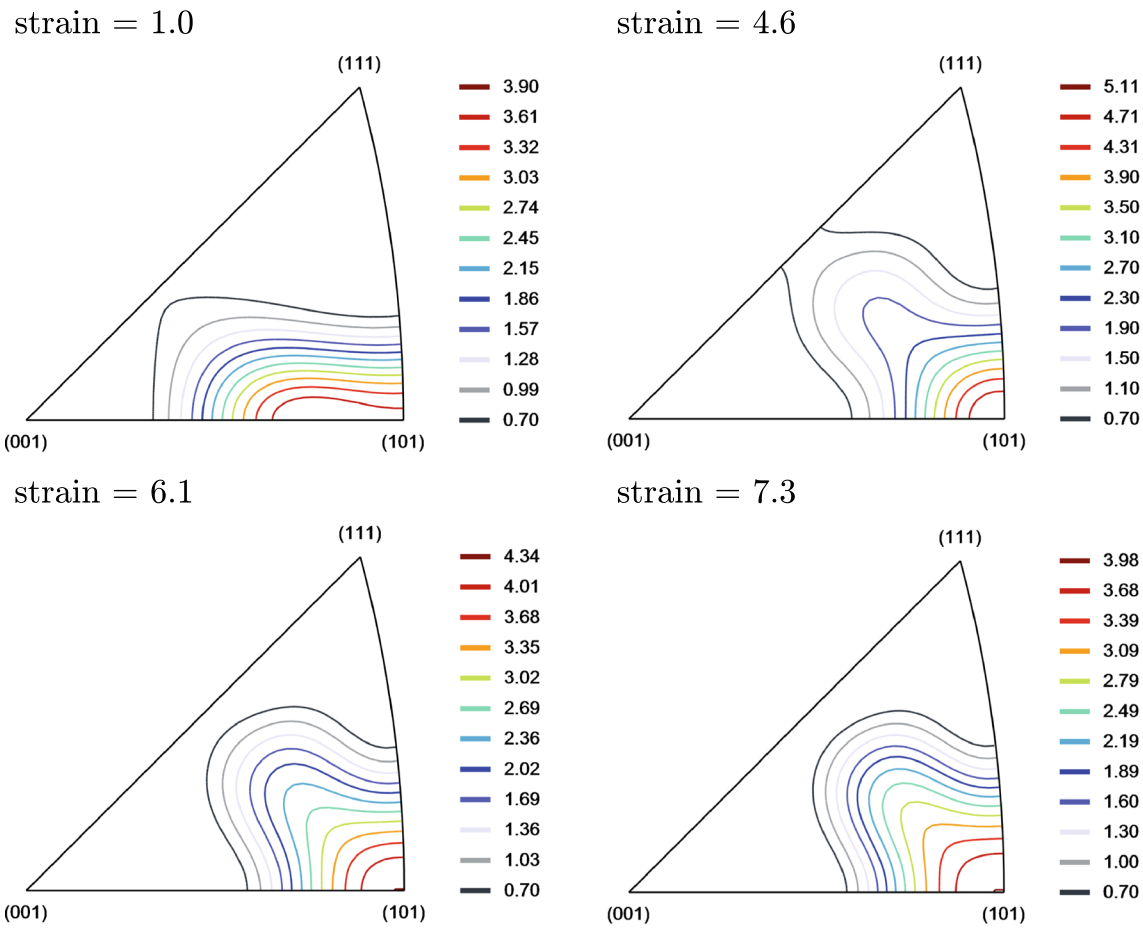

Fig. 2—The inverse pole figures for the rolling/swaging axis of the Fe-15 pct Cr binary ferritic alloy subjected to unidirectional deformation. The figures were plotted using the ATEX software.[40]

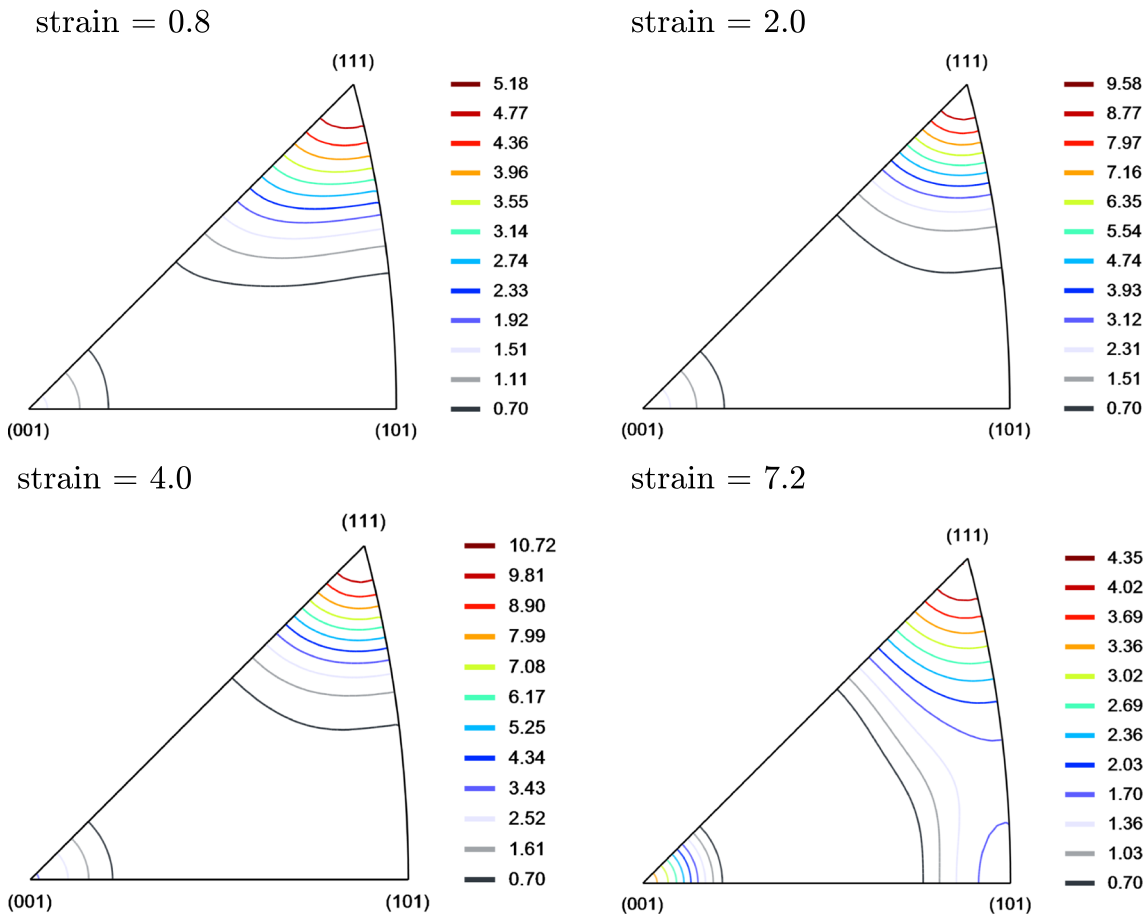

Fig. 3—The inverse pole figures for the last pass compression axis of the Fe-15 pct Cr binary ferritic alloy subjected to multidirectional deformation. The figures were plotted using the ATEX software.[40]

10, the cold rolling followed by swaging (unidirectional deformation mode) and the multidirectional compression through three orthogonal axes are simulated.

Figures 2 and 3 show the inverse pole figures obtained in the simulations of rolling/swaging (RS) and multidirectional forging (MF), respectively. They can be compared with Figures 6 and 7 in Reference 10. In the case of the unidirectional deformation, the model correctly predicted the domination of the ⟨110⟩ fiber. In the case of MF, the model also correctly captured the strong ⟨111⟩ fiber, although the intensity of ⟨001⟩ fiber is underestimated at low strains. It should be noted that due to lack of experimental data, the initial texture was set as random. It is highly probable that feeding the model with experimental texture that is in agreement with the experimental one would lead to yet better texture predictions.

Figure 4 shows the misorientation angle distributions obtained in the 3SCP simulation. The obtained distributions can be directly compared with Figure 4 in Reference 10. The experimentally measured fraction of HABs read from Figure 5 in the cited paper are shown in Table III. Very good qualitative agreement with experimental results is obtained. Indeed, the 3SCP model correctly predicts that unidirectional deformation leads to faster grain refinement than the multidirectional one. Interestingly, it slightly exaggerates the difference between processing conditions leading to higher and lower fractions of HABs, compared to the experimental data for the highest strain. In addition, similar to the one in the experiment, the evolution of the fraction of HABs in the high-strain regime slows down in the case of rolling/swaging (RS) and considerably increases in the case of the multiple forging (MF).

IV. DISCUSSION

A brief description on the importance of the modeling effort presented here follows. The author is aware that there are other models having the potential of modeling the continuous dynamic recrystallization in steels. However, to the best of author's knowledge, only two simulations[24,26] of misorientation angle distribution have been presented so far, and only in one, the results included also the textural evolution. The model used in Reference 24 is a very powerful and accurate tool; however, it is very computationally demanding, and the application of a supercomputer is required to perform the simulations.[25] On the other hand, the 3SCP model is very computationally efficient—the simulations presented here can be performed in less than one hour on a laptop computer. Despite the small amount of resources

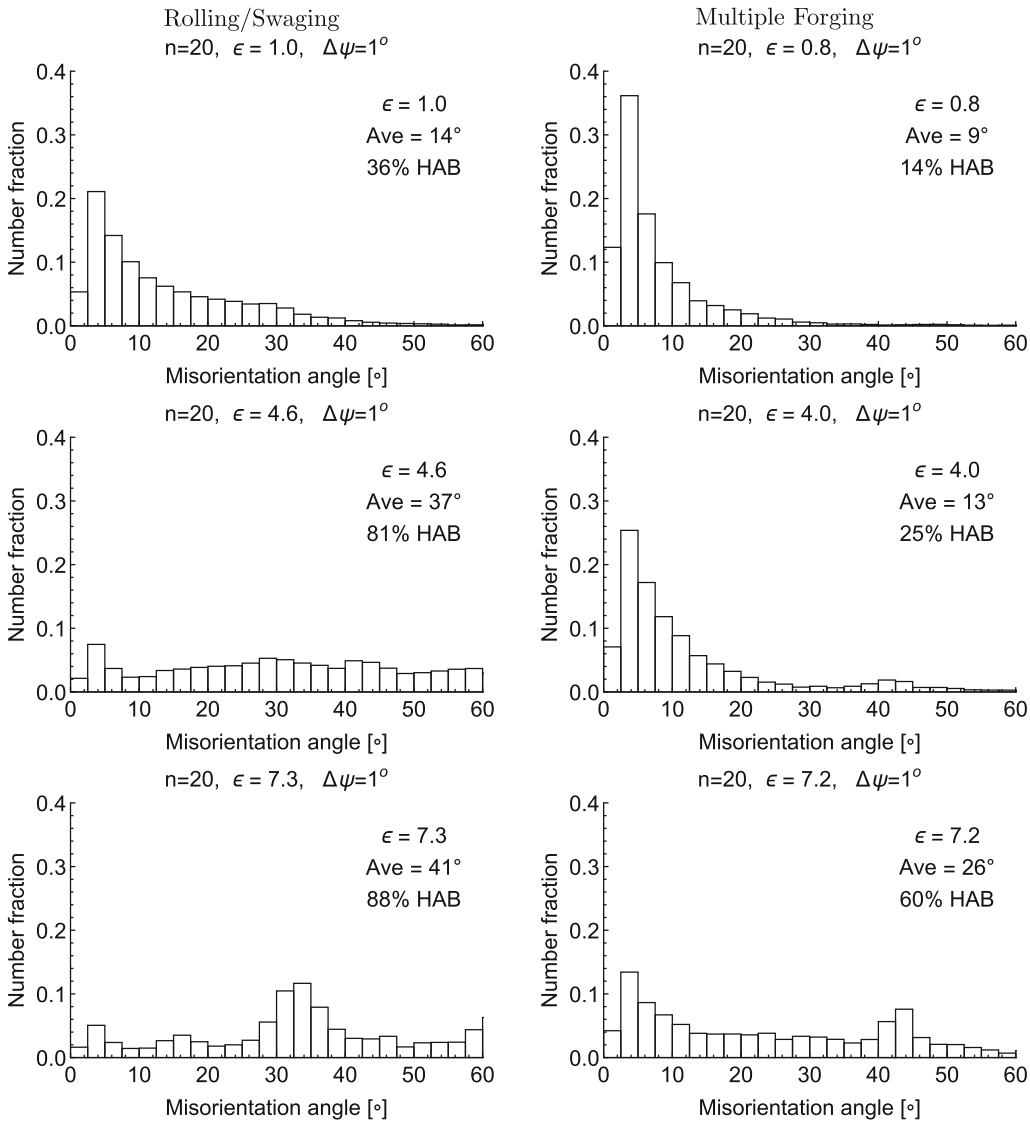

Fig. 4—The misorientation angle distributions calculated in the simulation of rolling/swaging and multiple forging applied to Fe-15 pct Cr ferritic stainless steel. The values of accumulated strain, average misorientation angle, and HAB fraction are shown in the plots.

Table III. The Fraction of High-Angle Boundaries (Pct) Read from Figure 5 in Ref. 10

Strain (RS/MF)	1.0/0.8	4.6/4.0	7.3/7.2
Rolling/Swaging (RS)	27	66	80
Multiple Forging (MF)	23	48	60

needed, the model is capable of predicting both texture and misorientation angle distributions in agreement with experimental data. Moreover, it can capture the differences in grain-refinement kinetics stemming from the change of deformation route.

It has already been shown in Reference 2 that increasing the value of rate-sensitivity parameter n leads to faster grain refinement in the 3SCP model. This can be easily explained by the fact that grain refinement in the model is driven by activities of different slip systems in different subgrains. Higher n leads to the situation where less slip systems can be simultaneously activated in the given crystal. Therefore, the driving force for the activation of different slip systems in different subgrains is higher since by this way the overall polycrystal deformation can be achieved. In contrast, when the n value is low, many slip systems can be activated in one subgrain simultaneously, and the driving force for the grain refinement is lower.

In Reference 41, the exponent in the power law was correlated with the stacking fault energy (SFE).[5] Austenitic iron has a low-to-medium SFE, while ferritic a high SFE. It is thus in accordance with this result that the experimental data are well predicted with $n = 15$ in the case of the 304 austenitic stainless steel and $n = 20$ in the case of the Fe-15 pct Cr ferritic stainless steel. Similar n-SFE dependence can be observed in the results published in Reference 2. There the 3SCP simulations of high-purity aluminum (high SFE) and its alloy with Mg (lower SFE) were conducted. It appeared that the

experimental results could be qualitatively well predicted using for both materials the same crystal plasticity parameters, but different n values equal to 20 and 10 in the case of high-purity metal and its alloy, respectively.

V. CONCLUSIONS

In this paper, the simulation of microstructural evolution of two steels subjected to large plastic deformation was described. It was shown that

1. the simulated misorientation angle distributions in the case of both FCC and BCC steels are in close agreement with experimental data;
2. the 3SCP model developed originally for FCC materials is applicable also to BCC alloy;
3. the value of the rate sensitivity exponent n has considerable impact upon the predicted kinetics of grain refinement;
4. the 3SCP model correctly predicts the influence of the processing route upon the grain-refinement kinetics; and
5. the 3SCP model is an attractive alternative to the existing models due to its computational efficiency and effectiveness in predictive capabilities.

ACKNOWLEDGMENTS

The author is grateful to Prof. Katarzyna Kowalczyk-Gajewska from IPPT PAN (Warsaw) for fruitful discussions. Special thanks are offered to Paweł Hołobut from IPPT PAN (Warsaw) for his help in the final language corrections. The research is supported by the project of the National Science Centre, Poland (NCN), under Grant No. 2016/23/B/ST8/03418.

OPEN ACCESS

REFERENCES

1. W. Burian, B. Garbarz: Pr. IMZ. 2009, vol. 61(1 s1). In Polish.
2. K. Frydrych and K. Kowalczyk-Gajewska: *Mater. Sci. Eng. A*, 2016, vol. 658, pp. 490–502.
3. K. Frydrych and K. Kowalczyk-Gajewska: *Model. Simul. Mater. Sci. Eng.*, 2018, vol. 26 (6), pp. 1–32.
4. R. Song, D. Ponge, D. Raabe, J.G. Speer, and D.K. Matlock: *Mater. Sci. Eng. A*, 2006, vol. 441 (1–2), pp. 1–17.
5. T. Sakai, A. Belyakov, R. Kaibyshev, H. Miura, and J.J. Jonas: *Prog. Mater. Sci.*, 2014, vol. 60, pp. 130–207.
6. K. Huang and R. Logé: *Mater. Des.*, 2016, vol. 111, pp. 548–74.
7. A. Belyakov, K. Tsuzaki, H. Miura, and T. Sakai: *Acta Mater.*, 2003, vol. 51 (3), pp. 847–61.
8. A. Belyakov, Y. Kimura, Y. Adachi, and K. Tsuzaki: *Mater. Trans.*, 2004, vol. 45 (9), pp. 2812–21.
9. A. Belyakov, Y. Kimura, and K. Tsuzaki: *Acta Mater.*, 2006, vol. 54 (9), pp. 2521–32.
10. A. Belyakov, K. Tsuzaki, Y. Kimura, Y. Kimura, and Y. Mishima: *Mater. Sci. Eng. A*, 2007, vol. 456 (1–2), pp. 323–31.
11. T. Sakai, A. Belyakov, and H. Miura: *Metall. Mater. Trans. A*, 2008, vol. 39 (9), pp. 2206–2214.
12. Y.E. Shakhova, Z.C. Yanushkevich, and A. Belyakov: *Russ. Metall.*, 2012, vol. 2012 (9), pp. 772–78.
13. M. Tikhonova, A. Belyakov, and R. Kaibyshev: *Mater. Sci. Eng. A*, 2013, vol. 564, pp. 413–22.
14. Z. Yanushkevich, A. Belyakov, and R. Kaibyshev: *Acta Mater.*, 2015, vol. 82, pp. 244–54.
15. M. Odnobokova, A. Belyakov, and R. Kaibyshev: *Metals*, 2015, vol. 5 (2), pp. 656–68.
16. N. Tsuji, Y. Saito, H. Utsunomiya, and S. Tanigawa: *Scr. Mater.*, 1999, vol. 40 (7), pp. 795–800.
17. N. Tsuji, S. Okuno, Y. Koizumi, and Y. Minamino: *Mater. Trans.*, 2004, vol. 45 (7), pp. 2272–81.
18. A. Kolahi, A. Akbarzadeh, and M. Barnett: *J. Mater. Process. Technol.*, 2009, vol. 209 (3), pp. 1436–44.
19. K. Rodak, J. Pawlicki, M. Tkocz: Mechanical and microstructural aspects of severe plastic deformation of austenitic steel. In: IOP Conf. Ser. Mater. Sci. Eng., 2012, vol. 35, p. 012008. IOP Publishing.
20. L. Longfei, Y. Wangyue, and S. Zuqing: *Metall. Mater. Trans. A*, 2006, vol. 37 (3), pp. 609–19.
21. R. Valiev, Y.V. Ivanisenko, E. Rauch, and B. Baudelet: *Acta Mater.*, 1996, vol. 44 (12), pp. 4705–12.
22. H. Petryk, S. Stupkiewicz, and R. Kuziak: *J. Mater. Process. Technol.*, 2008, vol. 204 (1–3), pp. 255–63.
23. H. Petryk and S. Stupkiewicz: *Mater. Sci. Eng. A*, 2007, vol. 444, pp. 214–19.
24. R. Lapovok, D. Orlov, I. Timokhina, A. Pougis, L. Toth, P. Hodgson, A. Haldar, and D. Bhattacharjee: *Metall. Mater. Trans. A*, 2012, vol. 43 (4), pp. 1328–40.
25. L.S. Toth, Y. Estrin, R. Lapovok, and C. Gu: *Acta Mater.*, 2010, vol. 58, pp. 1782–94.
26. D.S. Svyetlichnyy, K. Muszka, and J. Majta: *Comput. Mater. Sci.*, 2015, vol. 102, pp. 159–66.
27. K. Frydrych: Modelling of microstructure evolution of high specific strength metals subjected to severe plastic deformation processes. Ph.D. thesis, Institute of Fundamental Technological Research, Polish Academy of Sciences, Warsaw, Poland. 2011. in Polish.
28. K. Frydrych and K. Kowalczyk-Gajewska: *Metall. Mater. Trans. A*, 2018, vol. 49 (8), pp. 3610–23.
29. G.I. Taylor: *J. Inst. Met.*, 1938, vol. 62, pp. 307–24.
30. G. Sachs: *Z. VDI*, 1928, vol. 72, pp. 734–736.
31. A. Molinari, G.R. Canova, and S. Ahzi: *Acta Metall.*, 1987, vol. 35, pp. 2983–94.
32. R.A. Lebensohn and C.N. Tomé: *Acta Metall. Mater.*, 1993, vol. 41, pp. 2611–24.
33. K. Kowalczyk-Gajewska:Thermoplasticity of polycrystals in *Encyclopedia of Thermal Stresses*, R Hetnarski, ed., Springer, New York, 2014, pp. 6064–76.
34. K. Kowalczyk-Gajewska: IFTR Reports 1/2011. 2011, pp. 1–299.
35. A. Morawiec: *Orientations and Rotations. Computations in Crystallographic Textures*, Springer, Berlin, 2004.
36. K. Kowalczyk-Gajewska: *Eur. J. Mech. Solids A*, 2010, vol. 29, pp. 28–41.
37. R.J. Asaro and A. Needleman: *Acta Metall.*, 1985, vol. 33 (6), pp. 923–53.
38. L. Anand: *Comput. Methods Appl. Mech. Eng.*, 2004, vol. 193, pp. 5359–83.
39. K. Kowalczyk-Gajewska, Z. Mróz, and R.B. Pęcherski: *Arch. Metall. Mater.*, 2007, vol. 52, pp. 181–92.
40. B. Beausir, J.J. Fundenberger: (2018). http://atex-software.eu/.
41. W. Gambin and F. Barlat: *Int. J. Plast.*, 1997, vol. 13 (1/2), pp. 75–85.